nebulae luminosity functions (figures 18, 26 in ref. 26), if the population is typically older than 1 Gyr, then $t_{365} < 2$ Gyr. We therefore adopt $t < 3$ Gyr as a limit for most of the observed planetary nebulae in the four galaxies. This indicates an association with the "young" simulated stars, and that the mergers of gaseous disks are relevant to those ellipticals showing planetary nebulae. A caveat is the apparent relative invariance of the planetary-nebula luminosity function between galaxies, seemingly independent of signs for a recent major merger. When there are no such signs, the observed planetary nebulae may be the signature of recent minor mergers, which are expected to produce similar effects.

Received 27 January; accepted 22 June 2005.

1. Sofue, Y. & Rubin, V. Rotation curves of spiral galaxies. *Annu. Rev. Astron. Astrophys.* **39**, 137–174 (2001).
2. White, S. D. M. & Rees, M. J. Core condensation in heavy halos—A two-stage theory for galaxy formation and clustering. *Mon. Not. R. Astron. Soc.* **183**, 341–358 (1978).
3. Méndez, R. H. *et al.* Detection, photometry, and sitless radial velocities of 535 planetary nebulae in the flattened elliptical galaxy NGC 4697. *Astrophys. J.* **563**, 135–150 (2001).
4. Romanowsky, A. J. *et al.* A dearth of dark matter in ordinary elliptical galaxies. *Science* **301**, 1696–1698 (2003).
5. Cox, T. J. *Simulations of Galaxy Mergers: Star Formation and Feedback*. PhD thesis, UC Santa Cruz (2004); http://physics.ucsc.edu/~tj/work/thesis/.
6. Cox, T. J., Jonsson, P., Primack, J. R. & Somerville, R. S. The effects of feedback in simulations of disk galaxy major mergers. Preprint at (http://arXiv.org/astro-ph/0503201) (2005).
7. Navarro, J. F., Frenk, C. S. & White, S. D. M. A Universal Density Profile from Hierarchical Clustering. *Astrophys. J.* **490**, 493–510 (1997).
8. Blumenthal, G. R., Faber, S. M., Primack, J. R. & Rees, M. J. Formation of galaxies and large-scale structure with cold dark matter. *Nature* **311**, 517–525 (1984).
9. Dekel, A. & Silk, J. The origin of dwarf galaxies, cold dark matter, and biased galaxy formation. *Astrophys. J.* **303**, 39–55 (1986).
10. Fall, S. M. Dissipation, merging and the rotation of galaxies. *Nature* **281**, 200–202 (1979).
11. Mathews, W. G. & Brighenti, F. Hot gas in and around elliptical galaxies. *Annu. Rev. Astron. Astrophys.* **41**, 191–239 (2003).
12. Keeton, C. R. Cold dark matter and strong gravitational lensing: concord or conflict? *Astrophys. J.* **561**, 46–60 (2001).
13. Mamon, G. A. & Lokas, E. L. Dark matter in elliptical galaxies: II. Estimating the mass within the virial radius. *Mon. Not. R. Astron. Soc.* (in the press); preprint at (http://arXiv.org/astro-ph/0410489) (2005).
14. Napolitano, N. R. *et al.* Mass-to-light ratio gradients in early-type galaxy haloes. *Mon. Not. R. Astron. Soc.* **357**, 691–706 (2005).
15. Milgrom, M. & Sanders, R. H. Modified newtonian dynamics and the "dearth of dark matter in ordinary elliptical galaxies". *Astrophys. J. Lett.* **599**, L25–L28 (2003).
16. Valluri, M., Merritt, D. & Emsellem, E. Difficulties with recovering the masses of supermassive black holes from stellar kinematical data. *Astrophys. J.* **602**, 66–92 (2004).
17. Binney, J. & Tremaine, S. *Galactic Dynamics* Ch. 4.2.d, eq. 4–55 (Princeton Univ. Press, Princeton, NJ, 1987).
18. de Vaucouleurs, G. Recherches sur les Nebuleuses Extragalactiques. *Ann. Astrophys.* **11**, 247–287 (1948).
19. Lima Neto, G. B., Gerbal, D. & Marquez, I. The specific entropy of elliptical galaxies: an explanation for profile-shape distance indicators. *Mon. Not. R. Astron. Soc.* **309**, 481–495 (1999).
20. Bullock, J. S. *et al.* Profiles of dark haloes: evolution, scatter and environment. *Mon. Not. R. Astron. Soc.* **321**, 559–575 (2001).
21. Springel, V., Yoshida, N. & White, S. D. M. GADGET: a code for collisionless and gas dynamical cosmological simulations. *New Astron.* **6**, 79–117 (2001).
22. Gnedin, O. Y., Kravtsov, A. V., Klypin, A. A. & Nagai, D. Response of dark matter halos to condensation of baryons: cosmological simulations and improved adiabatic contraction model. *Astrophys. J.* **616**, 16–26 (2004).
23. Goudfrooij, P. *et al.* Interstellar matter in Shapley-Ames elliptical galaxies. I. Multicolour CCD surface photometry. *Astron. Astrophys. Suppl.* **104**, 179–231 (1994).
24. de Vaucouleurs, G. & Capaccioli, M. Luminosity distribution in galaxies. I—The elliptical galaxy NGC 3379 as a luminosity distribution standard. *Astrophys. J. Suppl.* **40**, 699–731 (1979).
25. Peletier, R. F., Davies, R. L., Illingworth, G. D., Davis, L. E. & Cawson, M. CCD surface photometry of galaxies with dynamical data. II—UBR photometry of 39 elliptical galaxies. *Astron. J.* **100**, 1091–1142 (1990).
26. Margo, P., Girardi, L., Weiss, A., Groenewegen, M. A. T. & Chinsi, C. Evolution of planetary nebulae. II. Population effects on the bright cut-off of the PNLF. *Astron. Astrophys.* **423**, 995–1015 (2004).
27. Peng, E. W., Ford, H. C. & Freeman, K. C. The planetary nebula system and dynamics in the outer halo of NGC 5128. *Astrophys. J.* **602**, 685–704 (2004).
28. Sáiz, A., Domínguez-Tenreiro, R. & Serna, A. Elliptical galaxies at $z = 0$ from self-consistent hydrodynamical simulations: comparison with Sloan Digital Sky Survey structural and kinematical data. *Astrophys. J. Lett.* **601**, L131–L134 (2004).
29. Abadi, M. G. Navarro, J. F. & Steinmetz, M. Stars beyond galaxies: The origin of extended luminous halos around galaxies. Preprint at (http://arXiv/astro-ph/0506659) (2005).
30. Côté, P. *et al.* Dynamics of the globular cluster system associated with M87 (NGC 4486). II. Analysis. *Astrophys. J.* **559**, 828–850 (2001).

Supplementary Information is linked to the online version of the paper at www.nature.com/nature.

Acknowledgements We acknowledge discussions with M. Beasley, A. Burkert, K. Gebhardt, J. Navarro, A. Romanowsky and his group, and assistance from M. Covington. This research has been supported by the Israel Science Foundation and by NASA and NSF at UCSC. The simulations were run at NERSC. A.D. acknowledges a Miller Professorship at UC Berkeley, support from UCO/Lick Observatory, and a Blaise Pascal International Chair in Paris.

Author Information Reprints and permissions information is available at npg.nature.com/reprintsandpermissions. The authors declare no competing financial interests. Correspondence and requests for materials should be addressed to A.D. (dekel@phys.huji.ac.il).

LETTERS

Isotope-induced partial localization of core electrons in the homonuclear molecule N_2

Daniel Rolles[1], Markus Braune[1], Slobodan Cvejanović[1]†, Oliver Geßner[1]†, Rainer Hentges[1], Sanja Korica[1], Burkhard Langer[2]†, Toralf Lischke[1]†, Georg Prümper[1]†, Axel Reinköster[1], Jens Viefhaus[1], Björn Zimmermann[3]†, Vincent McKoy[3] & Uwe Becker[1]

Because of inversion symmetry and particle exchange, all constituents of homonuclear diatomic molecules are in a quantum mechanically non-local coherent state; this includes the nuclei and deep-lying core electrons. Hence, the molecular photoemission can be regarded as a natural double-slit experiment[1]: coherent electron emission originates from two identical sites, and should give rise to characteristic interference patterns[2]. However, the quantum coherence is obscured if the two possible symmetry states of the electronic wavefunction ('*gerade*' and '*ungerade*') are degenerate; the sum of the two exactly resembles the distinguishable, incoherent emission from two localized core sites. Here we observe the coherence of core electrons in N_2 through a direct measurement of the interference exhibited in their emission. We also explore the gradual transition to a symmetry-broken system of localized electrons by comparing different isotope-substituted species—a phenomenon analogous to the acquisition of partial 'which-way' information in macroscopic double-slit experiments[3].

With respect to molecular inversion symmetry, the electronic wavefunctions of homonuclear diatomic molecules can be described as symmetry-adapted linear combinations of the corresponding atomic wavefunctions a and b, a situation actually realized by imposition of a fixed phase between them. For the core electrons, these symmetry-adapted wavefunctions Ψ, both *gerade* (*g*) and *ungerade* (*u*), can be written as:

$$\Psi_g = 1/\sqrt{[2(1+S)]} \times [\Psi_a(r) + \Psi_b(r)] \text{ and}$$

$$\Psi_u = 1/\sqrt{[2(1-S)]} \times [\Psi_a(r) - \Psi_b(r)]$$

respectively, where the phases of the two orbitals in Ψ_u differ by π and the overlap-integral is given by $S = \int \Psi_a(r)\Psi_b(r)dr$. The corresponding molecular orbitals for K-shell electrons are designated as $1\sigma_g$ and $1\sigma_u$.

The experimental fingerprint of the coherence of photoelectron emission from the $1\sigma_g$ and $1\sigma_u$ states in molecular nitrogen is the angular distributions in the molecular frame. These are predicted to exhibit characteristic differences between the two symmetry states, particularly in their nodal structure, which reflect the angular-momentum-dependent partial wave composition of the photoelectron wavefunction. In the non-local coherent case, this composition should be strictly governed by parity selection rules for the *gerade* and *ungerade* final core hole states, giving rise to purely odd and even angular momenta in the corresponding partial waves of the $1\sigma_g$ and $1\sigma_u$ photolines. The well-known alternating intensities in rotational spectra resulting from the symmetry that must be imposed on the nuclear spin function to make the complete eigenfunction of the molecule either symmetric or antisymmetric could be viewed as the nuclear analogue of this electronic selectivity behaviour. Replacing one particle in such a system by a different one leads to a complete breakdown of the symmetry properties of the system.

The showcase example for such complete change in behaviour is the rotational structure in homonuclear diatomic molecules under isotope substitution mentioned above. Here the symmetry selection rules totally collapse and all forbidden or suppressed rotational transitions become equally allowed[4]. On the other hand, the electronic charge distribution in such a molecule is virtually unchanged by isotope substitution. Indeed, according to the Born–Oppenheimer approximation with its complete decoupling of nuclear and electronic motion, no change should occur in the electronic wavefunction of a hetero-isotopic homonuclear molecule. Known violations of the symmetry rules for the ground vibrational and electronic state of homonuclear diatomic molecules are miniscule[5], and a symmetry breakdown has been observed for highly excited states only[6–9]. Hence, any observable isotope effects on the electronic wavefunction for core electrons, the key element for chemical and structural analysis of matter[10], might seem quite unexpected.

Here we show that inversion symmetry indeed causes non-local, coherent behaviour of the core electron photoemission from homonuclear diatomic molecules such as N_2 (ref. 11 and references therein). Our results show that this non-locality changes in a continuous way into partially localized behaviour, if inversion symmetry violations such as isotope substitution are induced.

The experiments were performed with vacuum ultraviolet synchrotron radiation from beamline BW3 of HASYLAB at DESY and beamline UE56/2-PGM1 and UE56/1-PGM at BESSY using a set of electron time-of-flight spectrometers in combination with an ion time-of-flight spectrometer with a position-sensitive anode (Fig. 1). This set-up makes it possible to determine all photoelectron and fragment ion momenta in coincidence, yielding, in the axial recoil approximation, the photoelectron angular distribution of fixed-in-space molecules[12,13]. Because the N_2:N(1*s*)-doublet splitting of less than 100 meV (ref. 14) had to be resolved while data were acquired over several days, these measurements required extremely high-energy resolution of both the beamline (40 meV) and our set-up (60 meV) as well as a very high photon beam stability, particularly regarding the photon energy (10^{-5}). Unresolved spectra would provide the sum of

[1]Fritz-Haber-Institut der Max-Planck-Gesellschaft, 14195 Berlin, Germany. [2]Max-Born-Institut für Nichtlineare Optik und Kurzzeitspektroskopie, 12489 Berlin, Germany. [3]California Institute of Technology, Pasadena, California 91125, USA. †Present addresses: Medical Faculty, Physics Department, University of Rijeka, 51000 Rijeka, Croatia (S.C.); Steacie Institute for Molecular Sciences, National Research Council Canada, Ottawa, Ontario K1A 0R6, Canada (O.G.); Institut für Physikalische Chemie, Universität Würzburg, 97074 Würzburg, Germany (B.L.); Institute of Multidisciplinary Research for Advanced Materials, Tohoku University, Sendai 980-8577, Japan (T.L. & G.P.); Max-Planck-Institut für Physik komplexer Systeme, 01187 Dresden, Germany (B.Z.).

the *gerade* and *ungerade* photoemission channels[15–19], which displays no effect of nonlocality of the core electrons.

Figure 2 shows the resolved molecule-frame angular distributions of the $1\sigma_g$ and $1\sigma_u$ photoelectrons, together with the angular difference arising from the interfering molecular charge distributions. Less characteristic, but still symmetry-specific behaviour occurs also in the non-coincident laboratory-frame angular distribution characterized by the photoelectron angular distribution parameter β (ref. 20) shown in Fig. 3. The distinction is particularly pronounced in the region of the trapped *f*-wave resonance at 9 eV above the N_2:N(1*s*) threshold because of the dominance of this *f*-partial continuum wave in only one (*gerade*) of the two photoelectron channels[21]. Note that the predicted crossover of the two *gerade* and *ungerade* angular distribution curves marks the onset of an oscillation driven by the spatial interference of the outgoing photoelectron.

We investigated the transition to the symmetry-broken system by comparing the naturally most abundant $^{14,14}N_2$ nitrogen molecule to two different isotopomers: singly substituted $^{14,15}N_2$ and doubly substituted $^{15,15}N_2$ (both 99% purity). Using the electron spectrometer in a non-coincident mode, that is, without detecting the corresponding fragment ions, we studied the effect of isotope substitution on the photoelectron spectrum. These effects are best illustrated in the ratio of the photoelectron spectra of normal and substituted nitrogen. Figure 4 shows the ratio between the 1*s* photoelectron spectra of normal $^{14,14}N_2$ and the isotopomer $^{14,15}N_2$ detected at the β-independent 'magic angle' ϑ_m (54.7°) with respect to the electric vector of the ionizing radiation as shown in Fig. 3), where the measured photoelectron intensity is directly proportional to the partial cross-section[20], as well as at 0° where the β-dependence is largest (see Fig. 3). The experimental data (purple circles) are shown together with a model calculation of the vibrational effect due to the mass-dependence of the vibrational constant (dashed black line in Fig. 4c and d), which causes nuclear-dynamics-dependent spectral changes.

We attribute the variation of the cross-sections and angular distributions beyond this behaviour to the breaking of inversion symmetry in the singly substituted species, which results in a partial localization of the core hole. Whereas the inversion symmetry of N_2 is preserved in the doubly substituted species $^{15,15}N_2$, the electronic wavefunction in $^{14,15}N_2$ is slightly modified owing to the broken symmetry of the singly substituted molecule, where the centre of symmetry r_{sm} of the electric charges midway between the two atoms no longer coincides with the centre of mass r_{cm} (ref. 8, 9). The wavefunctions in the molecule with broken inversion symmetry lose their character as parity eigenfunctions and can be described by linear combinations of the original *gerade* and *ungerade* wavefunctions. This mixing leads to greater similarity in the cross-sections and angular distributions, resulting in an isotope-induced effect in the range of a few per cent.

Two questions arise in this context: How may we understand the size of the observed effect, and why has it not been seen before in the photoelectron spectra of any homonuclear diatomic molecule? Both questions are closely related and require energy considerations related to the so-called diagonal and nondiagonal asymmetries in a bipolar system. (Here the terms 'diagonal' and 'nondiagonal' refer to contributions to the total hamiltonian of the system, which appear as diagonal and off-diagonal elements, respectively, when the origin of the coordinate system is equidistant from the two nuclei rather than at the centre of mass[8].) In $^{14,15}N_2$, the centre of mass r_{cm} is shifted away from the inversion centre r_{sm} by 1.7% of the bond length, resulting in 3.5% asymmetric motion per nucleus due to the

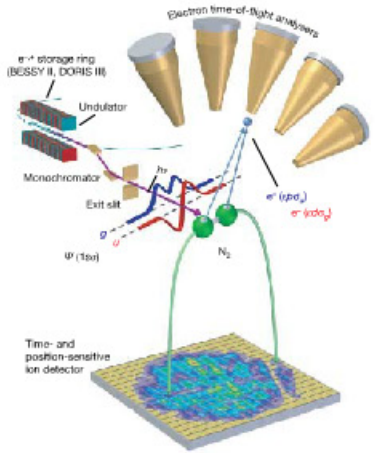

Figure 1 | Experimental set-up for a photoelectron-fragment ion coincidence experiment at a synchrotron radiation source. (For further details, see ref. 13.)

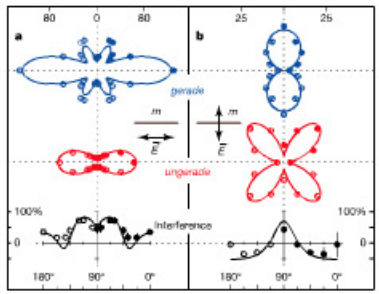

Figure 2 | Symmetry resolved photoelectron distributions in the molecule frame. Molecule frame photoelectron angular distributions (MPADs) for the *gerade* (upper panel) and *ungerade* (middle panel) N(1*s*) core photoelectron emission of N_2 at a photon energy of $h\nu = 419$ eV measured in the plane perpendicular to the light propagation direction for molecules oriented parallel (**a**) and perpendicular (**b**) to the light polarization vector through selection by an ion momentum resolving imaging detector. The fractional interference angular pattern shown in the lower panel are the differences between the *gerade* and *ungerade* MPADs divided by their respective sums $(g - u)/(g + u)$. The open circles are the mirror images of the measured data points (full circles), which are obtained by a least-squares fit of the coincident spectra. The error bars reflect the statistical uncertainty (s.d.) of the fit. The solid lines are predictions for non-local, coherent electron emission calculated in the partially relaxed core Hartree–Fock (RCHF) approximation[11] shown on a relative scale in arbitrary units marked at the upper margin, but unscaled with respect to each other. Note that the sensitivity of the measurements regarding the difference is considerably reduced at joint nodal points because of the low count rate in both transitions.

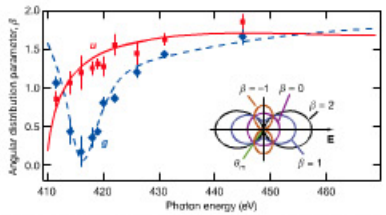

Figure 3 | Photoelectron angular distribution parameter β for N_2:N(1*s*) electron emission in the photon-energy range 410–450 eV. The symbols represent the experimental data for the *gerade* (blue diamonds) and *ungerade* (red squares) state. The error bars reflect the statistical and calibrational error. The results are compared to calculations in the partially RCHF approximation[11]. The dashed line shows the results for the *gerade* state, whereas the solid line represents the calculation for the *ungerade* state. Our RCHF curves are generally in good agreement with the data obtained by the Kohn–Sham density functional theory[12] and the random phase approximation[22] approach, in particular for the *ungerade* state (N. A. Cherepkov, personal communication).

relationship $r_{sm} = (m_{15} - m_{14})/(m_{15} + m_{14}) \times r_{iac}$, where m_{14} and m_{15} are the masses of ^{14}N and ^{15}N, which determines the time during which the electronic wave packet experiences asymmetric motion of the nuclei with respect to the inversion centre. This is similar to the inverse effect of symmetry restoration by detuned excitation in resonant inelastic X-ray scattering[22]. In dissociating systems, a loss of symmetry has been observed for autoionization[23] and resonant Auger[24] lines owing to the Doppler shift during the emission process.

A system of identical non-overlapping (that is, strongly localized) particles gives rise to completely degenerate *gerade* and *ungerade* states. Their underlying symmetry character is inaccessible to experimental exploration by photoelectron spectroscopy because the incoherent sums of *gerade* and *ungerade* states and of left- and right-hand states are, by definition, identical. A minimal delocalization resulting in a non-zero overlap between the two core orbitals is required to force a separation between the two symmetry-adapted states of the order of their natural lifetime width. Although this is just the case for N_2:N(1*s*) photoemission, other core level photoelectron spectra of diatomic homonuclear molecules do not fulfil this requirement[25].

In contrast to core levels, the *gerade* and *ungerade* splitting for valence levels is very large (in the range of several electron volts) owing to the strong delocalization of most valence electrons. In fact, all ground states are of *gerade* symmetry—the corresponding *ungerade* state is unoccupied. One may view the core level splitting in N_2 as being caused by a core valence-coupling-induced tunnelling rate giving rise to a roughly 15% probability that the electrons from one site will be at the other atomic site[25]. This tunnelling stabilizes the non-local, coherent character of the electronic state against asymmetric left/right, or, in our terminology, nondiagonal distortions such as a shift of the centre of mass away from the inversion centre, which, for small distortions, may be treated as a perturbation. With regard to localization, it is the ratio of the two associated energies that determines the size of isotope-induced effects in the photoelectron spectra of diatomic homonuclear molecules, analogous to the role of tunnelling versus correlation energy in a superfluid/Mott insulator transition[26].

Of all the energy effects caused by isotope substitution, we find that only one, the vibrational motion giving rise to an asymmetry energy of the order of several millielectronvolts, is of importance. All other effects, particularly hyperfine perturbations which cause *gerade*/*ungerade* symmetry breaking in highly excited states[6,7] and isotope shifts inducing predissociation in isotopomers[8,9], are in the microelectronvolt range. The observed effect can therefore be viewed as the diatomic analogue of symmetry breaking by vibronic coupling in triatomic molecules[27] owing to the asymmetric part of the vibrational motion (in the range of 10 meV). Comparing this 10-meV fraction of the vibrational energy with the *gerade*/*ungerade* splitting of 100 meV yields a *gerade*/*ungerade* mixing coefficient

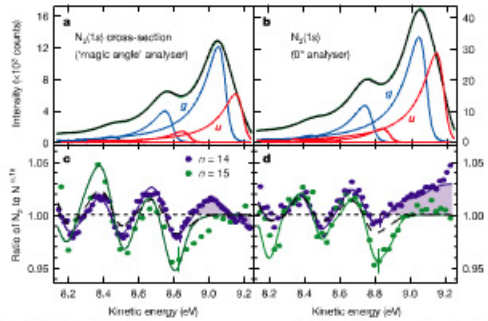

Figure 4 | Isotope effect on N_2. **a**, **b**, High-resolution photoelectron spectrum of $^{14,14}N_2$ recorded at a photon energy of $h\nu = 419$ eV at the β-independent 'magic angle' ϑ_m (left) and at 0° with respect to the polarization vector of the ionizing radiation (right). The error bars indicate the typical statistical error. The measured spectrum (green line) in the range of the 1*s* photoline is shown together with the unconvoluted representation of a least-squares fit of its two symmetry-components *gerade* (blue) and *ungerade* (red) and their respective vibrational progression up to the third vibrational level. **c**, **d**, Spectral ratio $^{14,14}N_2/^{14,15}N_2$ (purple) compared to $^{14,14}N_2/^{15,15}N_2$ (green) for the same angles as above. The solid lines are model calculations which include vibrational effects and, for $^{14,15}N_2$, the effect of symmetry breaking on the cross-sections. For $^{14,15}N_2$, the dashed line shows a model calculation of the vibrational effect only.

$[\Delta m/(m_{14}+m_{15})]/\Delta E_{gu}$ of 10%. To obtain the resulting relative change of the intensities in a first approximation, the square of the mixing coefficient must be multiplied by the normalized intensity difference of the *gerade* and *ungerade* channels $(I_g - I_u)/(I_g + I_u)$. At the photon energy considered here, this results in an estimated relative change of the cross-section of the order of 1%, which is consistent with the magnitude of the experimentally observed cross-section effect (Fig. 4c). The angle-dependent effect is enlarged owing to the role of the phase shifts between the photoelectron partial waves for all other emission directions besides the magic angle. It is worth mentioning that the size of the observed effect is still too small to be detected unambiguously in coincident measurements as shown in Fig. 2.

This analysis also explains why this effect has never been observed in valence photoionization, where the fractional size of the effect is more than two orders of magnitude smaller and where it must be measured on an absolute scale because there are no close-lying *gerade* and *ungerade* lines displaying effects in opposite directions. Such small absolute changes of less than 10^{-4} are inaccessible to photoelectron spectroscopy at present.

In summary, we have shown here that the inversion symmetry of a system indeed causes non-local, coherent behaviour of the otherwise localized core holes in homonuclear diatomic molecules such as N_2. This non-locality of the electron emission and the remaining core hole is neither conserved nor completely destroyed by a distinct symmetry distortion such as isotope substitution, but instead changes in a continuous way into partially localized behaviour owing to the gradual breakdown of inversion symmetry, as reflected by the loss of interference and parity mixing of the outgoing photoelectron waves. This isotope effect on the electronic structure of a diatomic molecule, probed here by photoelectron spectroscopy, is the first experimentally observed effect of its kind, to our knowledge.

The continuous nature of this transition, of which we have seen just the onset, makes it possible to control the character of a quantum state from either local or non-local by applying distinct forces that either stabilize or destabilize the non-locality. This knowledge might be useful in other systems such as double quantum dots, which are envisaged as the future building blocks of quantum gates[28,29].

With the advent of free-electron lasers (FEL)[30], which will permit time-resolved pump-probe experiments in the vacuum ultraviolet region, new experiments will become feasible that can probe transitions between complete localization of the electrons on individual atomic sites and complete non-localization over identical sites in analogy to the studies of coherence reported in reference[3]. To this end, we envision an experiment where a nitrous oxide (N_2O) molecule is broken into an O and a N_2 fragment by an initial light pulse and the core photoionization of the N_2 fragment is then probed for various time delays as the oxygen moves further and further away. With increasing distance, the emission characteristics should change from the localized, incoherent case of N_2O—where the two nitrogen atoms are distinct because of the chemical shift induced by the oxygen—to the non-local, coherent case of N_2.

METHODS

The model calculations shown in Fig. 4c and d are based on the results of a least-squares fit of the $^{14,14}N_2$ spectrum. The change of the vibrational constant is simulated by decreasing the energy spacing between the vibrational components by 5 meV, as predicted by a harmonic oscillator model. The symmetry-induced cross-section effect is modelled by further changing the intensity of the *gerade* and *ungerade* components. Changes to the Franck–Condon factors caused by the increased reduced mass of the substituted molecule are also included. However, they are found to be relatively small compared to the vibrational and cross-sectional effects. The increased mass leads to a decrease of the vibrational energy and therefore to pronounced oscillations in the intensity ratio, which coincide with the position of the vibrational progression. This vibrational effect should be more pronounced for the doubly substituted species $^{15,15}N_2$ owing to the larger change of its vibrational energy resulting from its heavier mass. The model calculation reproduces those oscillations very well, but fails to explain the additional 'wiggle' (shaded area) at the high-energy end of the $N_2^{14,15}N_2$ ratio, which is visible both in the ratio at the magic angle as well as at 0° with respect to the light polarization. This second effect, which does not appear in the $N_2^{15,15}N_2$ ratio (shown in green), can only be explained by a change in both relative intensity as well as angular distribution of the *gerade* and *ungerade* components in $^{14,15}N_2$ compared to the two other isotopomers. The model calculation including these changes (solid lines) reproduces the experimental data even at the high-energy end of the N_2:N(1s) photoline. It should be noted that the symmetry-induced effect is supposed to appear in all vibrational components; however, for the higher vibrational components below 8.9 eV, the symmetry effect tends to be masked by the vibrational effect. The pure symmetry effect is observed only in the lowest vibrational component above 9 eV.

Received 7 April; accepted 11 July 2005.

1. Lindner, F. *et al.* Attosecond double-slit experiment. *Phys. Rev. Lett.* **95,** 040401 (2005).
2. Briggs, J. S. & Walter, M. Oscillatory structure of molecular photoionisation cross-sections. *Phys. Essays* **13,** 297–302 (2000).
3. Hackermüller, L., Hornberger, K., Brezger, B., Zeilinger, A. & Arndt, M. Decoherence of matter waves by thermal emission of radiation. *Nature* **427,** 711–714 (2004).
4. Mulliken, R. S. Band spectra and atomic nuclei. *Trans. Faraday Soc.* **25,** 634–645 (1929).
5. Herzberg, G. *Molecular Spectra and Molecular Structure, Spectra of Diatomic Molecules* Vol. 1 139 (Krieger, Malabar, Florida, 1989).
6. Pique, J. P., Hartmann, F., Bacis, R., Churassy, S. & Koffend, J. B. Hyperfine-induced *ungerade-gerade* symmetry breaking in a homonuclear diatomic molecule near a dissociation limit: $^{127}I_2$ at the $^3P_{1/2}$–$^3P_{3/2}$ limit. *Phys. Rev. Lett.* **52,** 267–270 (1984).
7. Critchley, A. D. J., Hughes, A. N. & McNab, I. R. Direct measurement of a pure rotation transition in H_2. *Phys. Rev. Lett.* **86,** 1725–1728 (2001).
8. Cacciani, P. & Krakouline, V. Predissociation induced by *ungerade-gerade* symmetry breaking in $^6Li^7Li$ molecule. *Phys. Rev. Lett.* **84,** 5296–5299 (2000).
9. Bouloufa, N. *et al.* Predissociation induced by *ungerade-gerade* symmetry breaking in the $B^1\Pi_u$ state of the $^6Li^7Li$ molecule. *Phys. Rev. A* **63,** 042507 (2001).
10. Siegbahn, K., *et al. ESCA—Atomic, Molecular and Solid State Structure Studied by Means of Electron Spectroscopy* (Almqvist & Wiksells, Uppsala, 1967).
11. Broer, R. & Nieuwpoort, W. C. Hole localization and symmetry breaking. *J. Mol. Struct.* **458,** 19–25 (1999).
12. Heiser, F. *et al.* Demonstration of strong forward-backward asymmetry in the C1s photoelectron angular distribution from oriented CO molecules. *Phys. Rev. Lett.* **79,** 2435–2437 (1997).
13. Becker, U. Angle-resolved electron–electron and electron–ion coincidence spectroscopy: new tools for photoionization studies. *J. Electron. Spectrosc. Relat. Phenom.* **112,** 47–65 (2000).
14. Hergenhahn, U., Kugeler, O., Rüdel, A., Rennie, E. E. & Bradshaw, A. M. Symmetry-selective observation of the N 1s shape resonance in N_2. *J. Phys. Chem. A* **105,** 5704–5708 (2001).
15. Shigemasa, E. *et al.* Angular distributions of 1se photoelectrons from fixed-in-space N_2 molecules. *Phys. Rev. Lett.* **74,** 359–362 (1995).
16. Pavlychev, A. A. *et al.* Dynamic properties of N and O 1s σ_u shape resonances in N_2 and CO_2 molecules. *Phys. Rev. Lett.* **81,** 3623–3626 (1998).
17. Cherepkov, N. A. *et al.* Manifestation of many-electron correlations in photoionization of the K shell of N_2. *Phys. Rev. Lett.* **84,** 250–253 (2000).
18. Jahnke, T. *et al.* Circular dichroism in K-shell ionization from fixed-in-space CO and N_2 molecules. *Phys. Rev. Lett.* **88,** 073002 (2002).
19. Weber, Th. *et al.* K-shell photoionization of CO and N_2: is there a link between the photoelectron angular distribution and the molecular decay dynamics? *J. Phys. B* **34,** 3669–3678 (2001).
20. Yang, C. N. On the angular distribution in nuclear reactions and coincidence measurements. *Phys. Rev.* **74,** 764–772 (1948).
21. Dehmer, J. L. & Dill, D. Shape resonances in K-shell photoionization of diatomic molecules. *Phys. Rev. Lett.* **35,** 213–215 (1975).
22. Skytt, P. *et al.* Quenching of symmetry breaking in resonant inelastic X-ray scattering by detuned excitation. *Phys. Rev. Lett.* **77,** 5035–5038 (1996).
23. Golovin, A. V. *et al.* Observation of site-specific electron emission in the decay of superexcited O_2. *Phys. Rev. Lett.* **79,** 4554–4557 (1997).
24. Björneholm, O. *et al.* Doppler splitting of in-flight auger decay of dissociating oxygen molecules: the localization of delocalized core holes. *Phys. Rev. Lett.* **84,** 2826–2829 (2000).
25. Kosugi, N. Spin-orbit and exchange interactions in molecular inner shell spectroscopy. *J. Electron. Spectrosc. Relat. Phenom.* **137–140,** 335–343 (2004).
26. Greiner, M., Mandel, O., Esslinger, T., Hänsch, T. W. & Bloch, I. Quantum phase transition from a superfluid to a Mott insulator in a gas of ultracold atoms. *Nature* **415,** 39–44 (2002).
27. Domcke, W. & Cederbaum, L. S. Vibronic coupling and symmetry breaking in core electron ionization. *Chem. Phys.* **25,** 189–196 (1977).
28. Bayer, M. *et al.* Coupling and entangling of quantum states in quantum dot molecules. *Science* **291,** 451–453 (2001).
29. Hayashi, T., Fujisawa, T., Cheong, H. D., Jeong, Y. H. & Hirayama, Y. Coherent manipulation of electronic states in a double quantum dot. *Phys. Rev. Lett.* **91,** 226804 (2003).
30. Wabnitz, H. *et al.* Multiple ionization of atom clusters by intense soft X-rays from a free-electron laser. *Nature* **420,** 482–485 (2002).
31. Zimmermann, B., Wang, K. & McKoy, V. Circular dichroism in K-shell ionization from fixed-in-space CO and N_2. *Phys. Rev. A* **67,** 042711 (2003).
32. Stener, M., Fronzoni, G. & Decleva, P. Time dependent density functional study of the symmetry resolved N 1s photoionization in N_2. *Chem. Phys. Lett.* **351,** 469–474 (2002).
33. Semenov, S. K. & Cherepkov, N. A. Generalization of atomic random-phase-approximation method for diatomic molecules. II. N_2 K-shell photoionization. *Phys. Rev. A* **66,** 022708 (2002).

Acknowledgements We thank J. Bozek, R. Díez Muiño, F. J. García de Abajo, C. S. Fadley and M. A. Van Hove for many discussions about core-hole delocalization and coherent photoelectron emission in homonuclear molecules. The assistance of R. Püttner and F. Gelmukhanov in the interpretation of the effect of isotope substitution on the vibrational structure and the Franck–Condon factors is also acknowledged. The work was partly supported by the Bundesministerium für Bildung und Forschung (BMBF) and the Alexander von Humboldt Foundation (B.Z.).

Author Information Reprints and permissions information is available at npg.nature.com/reprintsandpermissions. The authors declare no competing financial interests. Correspondence and requests for materials should be addressed to U.B. (becker_u@fhi-berlin.mpg.de).